Desalination and Water Treatment
www.deswater.com
doi: 10.5004/dwt.2023.30216

316 (2023) 755–768
December

Leachate treatment by ceramic ultrafiltration membranes: fouling mechanisms identification

M. Farah[a,*], F.Z. Addar[a], S. Kitanou[a,b], M. Belfaquir[a], M. Tahaikt[a], M. Taky[a], A. Elmidaoui[a]

[a]*Laboratory of Advanced Materials and Process Engineering, Faculty of Sciences, Ibn Tofail University, BP 1246, Kenitra, Morocco, emails: mohamed.farah@uit.ac.ma (M. Farah), Fatima.zahra@uit.ac.ma (F.Z. Addar), Sarra.kitanou@uit.ac.ma (S. Kitanou), Belfaquir.mustapha@uit.ac.ma (M. Belfaquir), mustapha.tahaikt@uit.ac.ma (M. Tahaikt), elmidaoui@uit.ac.ma (A. Elmidaoui), mohamed.taky@uit.ac.ma. (M. Taky)*
[b]*National High School of Chemistry, Ibn Tofail University, Kenitra, Morocco*

Received 23 July 2023; Accepted 7 December 2023

ABSTRACT

The treatment of leachate is a complex process that involves the use of various treatment methods in order to achieve acceptable quality levels. The objective of this study is to investigate the impact of transmembrane pressure (TMP) at a constant flow velocity (V = 2m/s) on the treatment of leachate from the controlled landfill of Oum Azza, Rabat, Morocco, as well as on the fouling mechanism of three ultrafiltration (UF) ceramic membranes (UF20, UF50, and UF100) with varying porosities of 20, 50, and 100 nm. The experiments were conducted using a semi-industrial pilot plant provided by the French Company TIA (Techniques Industrielles Appliquées), which was equipped with a ceramic membrane. Two mathematical models, the Hermia model and the Bolton model, were used to identify the fouling mechanisms of the tested membranes. The Hermia model provides four equations that describe the four fouling modes, namely cake formation, intermediate blockage, pore constriction, and complete blockage. Furthermore, the Bolton model combines these fouling mechanisms to determine whether fouling is caused by adsorption, occlusion, or compression of the filter layer. The results indicate that the permeate and rejection of pollution indicators (chemical oxygen demand, 5-day biochemical oxygen demand, and total suspended solids) for the three tested membranes are affected by the TMP. The UF20 membrane showed the best rejection rates, followed by UF50 and finally UF100. For permeate flow, UF100 > UF50 > UF20. According to the Hermia model, the fouling of all three membranes was superficial, with the main fouling mechanisms being cake formation or intermediate blockage. Application of the Bolton model equations revealed that fouling of the UF20 and UF50 membranes was described by the combined equation of cake formation and complete blockage. For the UF100 membrane, fouling was described by the combined equation of cake formation and intermediate blockage.

Keywords: Ultrafiltration; Leachate; Ceramic membrane fouling; Modeling; Hermia model; Bolton model; Transmembrane pressure

1. Introduction

Leachate is a liquid that forms as a result of water percolating through waste in landfills and solubilizing both organic and inorganic compounds, especially after precipitation [1]. It is typically characterized by its dark color and strong odor, as well as its high organic and inorganic loads. Leachate contains an aqueous solution that includes four categories of pollutants: dissolved organic matter (including volatile fatty acids and more refractory organic matter such as humic substances), macro inorganic compounds (such as Ca^{2+}, Mg^{2+}, Na^{+}, K^{+}, NH_4^{+}, Fe^{2+}, Mn^{2+}, and HCO_3^{-}),

* Corresponding author.

heavy metals (such as Cd^{2+}, Cr^{3+}, Cu^{2+}, Pb^{2+}, and Ni^{2+}), aromatic hydrocarbons, phenols, and pesticides [2]. These pollutants can cause significant environmental harm due to their high levels of toxicity. Various methods have been explored to effectively treat landfill leachate, including biological treatment, chemical precipitation, chemical oxidation. Coagulation–flocculation, and membrane processes [3–8].

Several membrane solutions have been developed for the treatment of landfill leachate, including high-pressure techniques like reverse osmosis (RO) and nanofiltration (NF), which are effective in removing refractory chemical oxygen demand (COD). However, these techniques are generally considered too expensive for widespread use in most countries due to their high energy consumption [9]. On the other hand, low-pressure techniques such as microfiltration (MF) are less expensive but are not effective when used alone since they only remove colloids and suspended solids [10]. Ultrafiltration (UF), another low-pressure technique, can remove high molecular weight ingredients containing both biodegradable organic macromolecules and non-biodegradable substances but allows salinity to pass through [11]. However, membrane fouling caused by the organic pollution load of leachate results in frequent shutdowns for washing and reduces the lifespan of membranes. A thorough pretreatment can be implemented to address this issue. One promising method for removing suspended organic matter is UF, particularly with the use of new ceramic membranes.

Ceramic porous membranes have gained increasing popularity in industrial fields due to their high hydraulic permeability and narrow pore size distribution, superior to polymeric membranes with similar separation properties. They also exhibit exceptional chemical, mechanical, and thermal stability, the ability to undergo steam sterilization and backflushing, good erosion resistance, high fluxes per unit membrane area, high durability, resistance to bacterial attack and biological degradation, the potential for regeneration, and dry storage after cleaning [12–15]. These membranes are widely used in harsh environmental applications, such as oil/water separation, mining, textiles, petrochemicals, pharmaceuticals and biotechnology, and the food and beverage industry [16,17].

However, the main issue with UF operation is concentration polarization and membrane fouling, which can lead to decreased permeate flux.

Several mathematical models have been developed to describe the mechanisms of pore blockage and cake layer fouling caused by contaminants during the filtration process [18]. One of these models is Hermia, which was modified by Hermia [19] and Field et al. [20] and proposes four equations to describe the mechanisms, namely pore constriction, complete blockage, intermediate blockage, and cake formation.

The evolution of research on fouling models has led to the development of more comprehensive models that explain both the initial membrane pore blockage and the subsequent cake layer. For example, Ho and Zydney [21] presented a combined model that considers both mechanisms. Furthermore, Bolton et al. [22], by combining simple models in pairs, developed five models that consider different mechanisms: cake formation and complete blockage, cake formation and intermediate blockage, pore constriction and complete blockage, intermediate blockage and pore constriction, and cake formation and pore constriction. These models represent a significant advancement in comprehending and predicting fouling in membrane filtration processes.

Several studies have used the Hermia model to investigate fouling mechanisms in UF processes. For example, Gomes et al. [23] investigated the separation and purification of biodiesel produced by alkaline ethyl transesterification, using ceramic UF membranes with different pore sizes (0.2 μm, 0.1 μm, 0.05 μm, and 20 kDa) and TMP (1.2 and 3 bar). The Hermia model was used to identify the fouling mechanism, which was found to be complete pore blockage. Tomczak and Gryta [24] studied the separation of oily wastewater generated during marine transportation using an ultrafiltration ceramic membrane (8 kDa) under various conditions, including temperature (303 and 323 K), tangential flow rate (2.9–8.2 m/s), and TMP (0.28–0.40 MPa). The Hermia model was also used in this study to evaluate the fouling phenomenon, and it was found that the cake formation model was most consistent with the experimental data. Birrenbach et al. [25] investigated cross-flow ultrafiltration of ovalbumin aggregates with a 50 nm cut-off ceramic membrane, monitoring flow at different TMP and concentrations. The most significant fouling mechanism observed was intermediate pore blockage, which was best described by the Hermia model. Finally, Aloulou et al. [26] determined the optimal conditions for the treatment of industrial wastewater containing oil and heavy metals using a 150 kDa ultrafiltration ceramic membrane. The Hermia model was employed to estimate the fouling mechanism, and the results indicated that the decrease in permeate flux over time could be described by the cake filtration model. Modeling and optimization revealed that the best operating conditions were an initial oil concentration of 117 g/L and a feed temperature of 60°C, under a TMP of 3.5 bar.

Collado et al. [27] studied the potential of a tubular ultrafiltration membrane composed of titanium-zirconia (ZrO_2-TiO_2) in the treatment of two distinct types of leachates, one mature and the other young, from the La Zoreda landfill in Asturias, Spain. The experiments were carried out with a TMP of 1.6 bar and a transverse flow velocity of 3.2 m/s. The results of the study revealed that COD removal for mature leachates was 49.6% at a volumetric concentration factor (VCF) of 1.7. In contrast, under the same conditions, COD reduction for young leachates was 48%. In addition, the Hermia model demonstrated that the membrane fouling mechanism is of the cake-forming type.

Shi et al. [28] conducted a study on sugarcane juice clarification using a ceramic membrane with pore size of 20 nm. The researchers evaluated several pretreatment options, including heating the juice to different temperatures (60°C, 75°C, and 90°C) with and without sedimentation, and using the evaporator-supplied juice at different pH values (7.2, 7.5 and 7.8). In this study, the transmembrane pressure (TMP) was optimized between 0.1 and 0.3 MPa at a temperature of 75°C and a flow velocity of 3.5 m/s. The results showed that the best juice quality was obtained at a TMP of 0.026 MPa and a pH of 7.5. According to use of Bolton's combined

models, the fouling mechanism of partially clarified juice filtration results from a combination of cake filtration and complete blockage models. This study emphasizes the importance of considering both mechanisms when analyzing fouling, as they can affect the quality of clarified juice.

The objective of this study is to examine the effect of TMP and membrane porosity on permeate quality during leachate treatment. The tested ultrafiltration membranes are made of ceramic with porosities of 20, 50 and 100 nm. The identification of fouling mechanisms involved was carried out using two mathematical models, the Hermia model and the Bolton model. For this purpose, the permeate flux was monitored over time, as well as the physico-chemical quality of the permeate. This work aims to provide information on the fouling behavior of ceramic membranes as a function of TMP and to offer a better understanding of the effect of TMP on permeate quality during leachate treatment.

2. Materials and methods

2.1. Experimental method

2.1.1. Experimental feed solution

Leachate from the Oum Azza site was used in this study. The samples collected were transported to the laboratory for analysis and treatment within hours of collection. The physico-chemical characteristics of the leachates are presented in Table 1.

2.1.2. Membrane characterization

Experiments are performed on a UF laboratory pilot supplied by the French Company TIA (Techniques Industrielles Appliquées). It consists of a feeding tray with a capacity of 50 L and two pumps: one for circulation and the other for filtration (Fig. 1). The tangential velocity of recirculation is in the range 0.5–6 m/s. The TMP varies from 0 to 10 bar. Table 2 gives the main characteristics of the UF membranes used.

2.1.3. UF operation on leachate solution

To investigate the influence of operating conditions on membrane fouling and permeate quality. UF experiments using three ultrafiltration membranes (UF20, UF50, and UF100) have carried out at constant velocity (CV) constant of 2 m/s and different PTMs (1, 2, 3 and 4 bar). All experiments are performed at a temperature of 25°C. The retentate flow is recirculated into the feed tank and the permeate flow is monitored throughout the UF experiments as a function of time, a sample is taken at the beginning of the operation and then every 5 L of the permeate, a sample is taken for analysis.

2.1.4. Membrane cleaning procedure

After each UF operation, the membrane is subjected to a cleaning cycle that consists first of a rinse with tap water for 20 min then an alkaline cleaning with an aqueous NaOH solution (pH between 11 and 12) for 30 min and finally, after the rinse, a last acidic cleaning with an aqueous sulfuric acid solution (pH between 2 and 3) for 20 min followed by a final rinse of the membrane with tap water until the pH of the water becomes neutral. The procedure is repeated as many times as necessary until the initial permeability is recovered. All cleaning steps, including rinses, are performed at a CV of 2 m/s and an TMP of 1 bar. Once the membrane is cleaned, the water permeability is verified.

2.1.5. Analytical measurements

Permeate samples were collected and leachate parameters were determined analytically using standard methods. The analyses of chemical oxygen demand (NF T90-101), 5-d biochemical oxygen demand (BOD_5 - NF T90-103) and

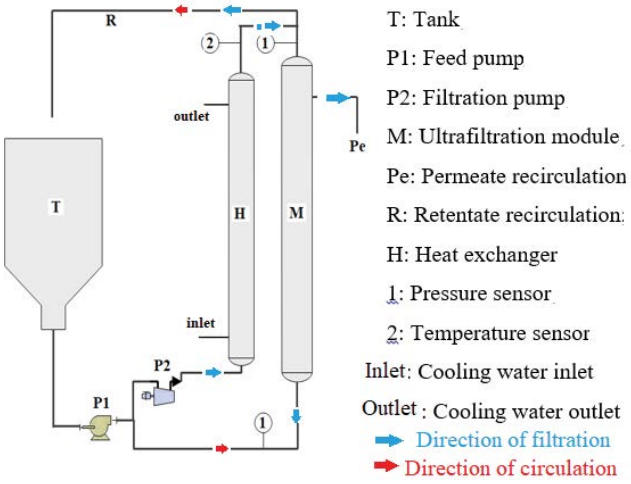

Fig. 1. Diagram of the ultrafiltration pilot plant.

Table 1
Physico-chemical and organic characterization of Oum Azza leachates

Parameter	Value
pH	8.5 ± 0.2
T (°C)	18.6
Electric conductivity (mS/cm)	30 ± 3
Chemical oxygen demand (mg/L)	8,000 ± 2,000
5-d biochemical oxygen demand (mg/L)	4,500 ± 1,000
Total suspended solids (mg/L)	4,120 ± 1,000

Table 2
Characteristics of the membranes

Characteristics	UF20	UF50	UF100
Pore size (nm)	20	50	100
Nature	Ceramic	Ceramic	Ceramic
Surface (m^2)	0.35	0.35	0.24
Maximum pressure (bar)	10	10	10
Maximum temperature (°C)	100	100	100
pH range	3–11	3–11	3–11

total suspended solids (TSS - NF T90-105-2) are conducted in accordance with the AFNOR Standard (1997) [29]:

COD assesses the total amount of oxygen required for the chemical oxidation reaction of organic matter in a water sample. This measurement is performed by exposing the sample to a potent oxidizing agent, typically a mixture of potassium dichromate and sulfuric acid, at a high temperature. The reduction in the color of the solution, resulting from the consumption of the oxidant, is then measured to calculate COD.

BOD_5 quantifies the amount of oxygen consumed by microorganisms during the decomposition of organic matter in water over a 5-day period. The water sample is incubated at a constant temperature, usually 20°C during this period. The decrease in dissolved oxygen over time is measured and used to determine BOD_5.

TSS, it assesses the quantity of particles suspended in water. To achieve this, the sample is filtered through a specific filter, the retained particles are then dried and weighed. The obtained mass is then used to express the concentration of suspended solids in the water.

The retention (R) is calculated as a percentage according to Eq. (1):

$$R(\%) = \frac{C_0 - C_p}{C_0} \times 100 \quad (1)$$

where C_p and C_0 are permeate and initial concentrations, respectively.

3. Results and discussions

3.1. Effect of TMP on permeate flux and leachate parameters

3.1.1. On the permeate flux

The effects of TMP on permeate flux were examined for three different membranes at a CV of 2 m/s. The temporal evolution of the permeate flux is described in Fig. 2. In addition, Table 3 shows the limiting fluxes and flux drop rate for the three membranes at different TMP.

After analyzing Fig. 2 and Table 3, it is evident that the permeate flux experiences a decline over time for all three

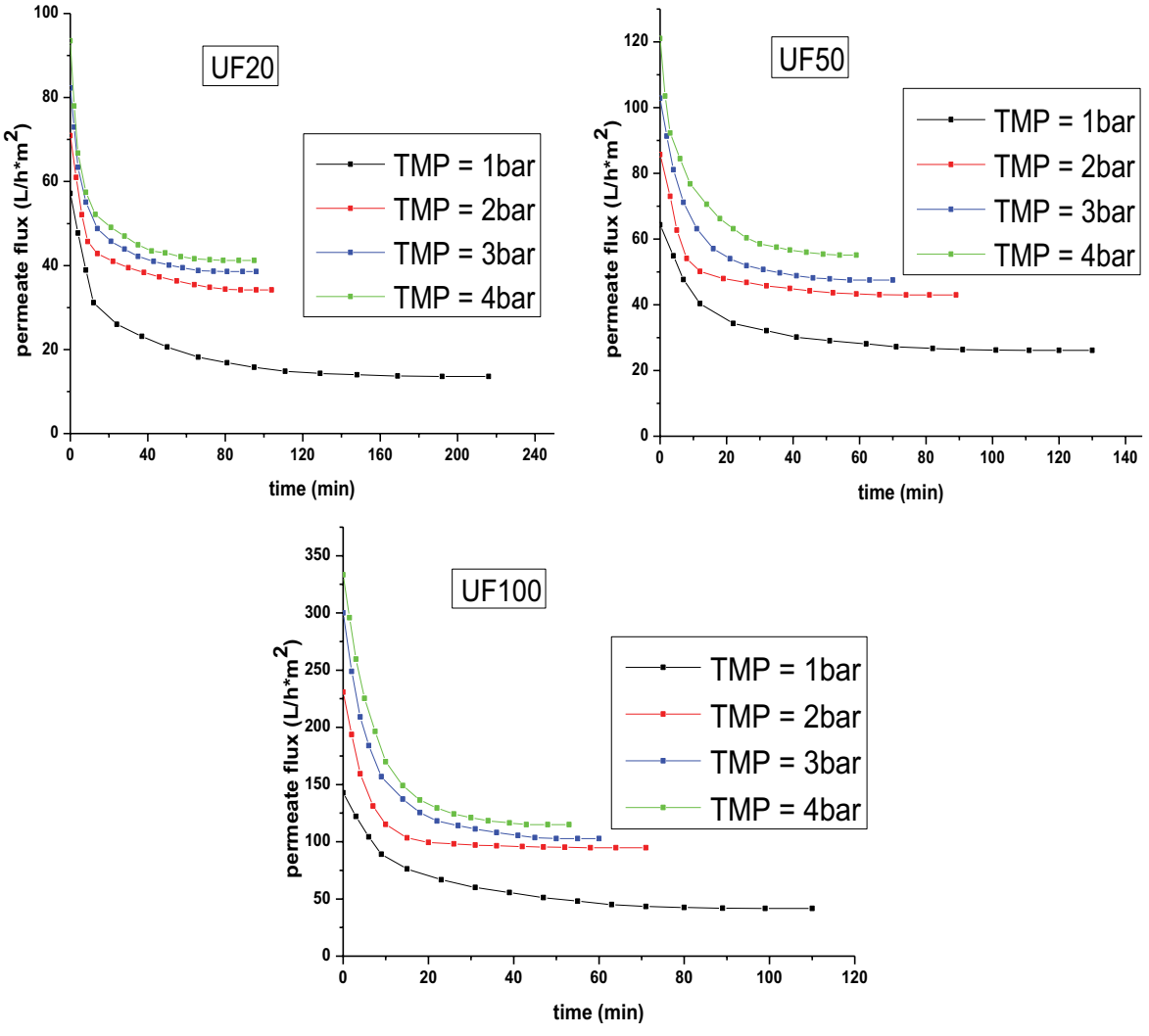

Fig. 2. Variation of permeate flux as a function of time for the three membranes.

Table 3
Flux limits and flux drop rate for the three membranes

	TMP = 1 bar		TMP = 2 bar		TMP = 3 bar		TMP = 4 bar	
	Flux limits ($L/h \cdot m^2$)	Flux drop	Flux limits ($L/h \cdot m^2$)	Flux drop	Flux limits ($L/h \cdot m^2$)	Flux drop	Flux limits ($L/h \cdot m^2$)	Flux drop
UF20	13.61	76.18%	34.19	51.78%	38.55	53.14%	41.19	55.93%
UF50	26.12	59.36%	42.99	49.84%	47.5	53.81%	55.09	54.47%
UF100	41.66	70.83%	94.8	58.91%	102.8	65.73%	114.9	65.52%

UF membranes and various applied TMPs. This decline occurs in three stages: the first stage demonstrates a significant drop in permeate flux due to concentration polarization, followed by a gradual decrease in the second stage until the flux level matches the beginning of fouling. The third stage of the curve signifies a stagnant or limiting flux due to complete fouling. Additionally, Fig. 2 illustrates that the permeate flux obtained from the UF membranes is dependent on their porosity. As the membrane pore radius increases, the permeate flux increases in the following order: UF100 > UF50 > UF20.

The permeate flux and limit flux of all three membranes are influenced by the TMP. As the TMP increases, both the permeate flux and limit flux increase, resulting in a decrease in the drop in permeate flux. The limit flux is explained by the gel polarization model, which suggests that the concentration polarization phenomenon occurs when the feed solution containing suspended and soluble solids (colloids) passes through the membrane. This creates a viscous, gelatinous layer that adds resistance to the permeate flow, in addition to the membrane's resistance [30]. The film model indicates that increasing the TMP improves the hydrodynamic conditions, mitigating the concentration bias effect, and preventing the fouling layer's formation. This leads to an increase in permeate flux and an improvement in the mass transfer coefficient [31,32]. The phenomenon can be explained by the following:

- The increase in pressure changes the structure of the particle deposit.
- The increase in pressure causes particles of different sizes to rise to the surface, forming a more compact and less porous cake.
- The increase in pressure favors the penetration of particles inside the pores of the membrane, which reduces their size [33,34].

Membrane fouling results from intricate physical and chemical interactions among various pollutants in the food supply and between these compounds and the membrane surface. These substances can bind, accumulate, or adsorb on membrane surfaces or within membrane pores due to mass transfer, leading to fouling. Various factors, such as the concentration and nature of the feed solution, temperature, membrane properties (surface morphology, hydrophobicity, charge, and molecular weight cutoff), mode of operation, and hydrodynamic conditions, including initial permeate flow rate and cross flow velocity, can collectively influence overall membrane performance and fouling propensity. Additionally, factors altering or impacting the hydrodynamic conditions of membrane modules and the properties of the feed solution can influence membrane performance and fouling, as indicated by various studies [35–37]. Nevertheless, TMP and flow speed remain pivotal in the fouling of ultrafiltration membranes. In the pre-gel phase of TMP, the flow rate exhibits a linear increase until it reaches a pressure-independent flow limit. However, the formation of the fouling layer, especially under high pressures, leads to compression and subsequent reduction in flow. Flow velocity enhances hydrodynamic conditions, reducing the thickness of the concentration polarization layer. This reduction facilitates an efficient turnover of leachate, delaying concentration polarization and improving the mass transfer coefficient, ultimately resulting in an increase in permeate flux, fouling becomes a competition between flow velocity and TMP. To mitigate fouling, achieving a delicate balance between these two parameters is crucial. In our study, the applied circulation speed proved effective for TMPs of 1 and 2 bars. However, at TMPs exceeding 2 bars, the TMP takes precedence, indicating the need to increase circulation speed under such conditions. This finding aligns with research by Zait et al. [29], demonstrating that flow velocity and TMP significantly impact the flow limit, emphasizing an increased need for flow velocity at higher pressures.

3.1.2. On the treated leachate parameters

Fig. 3 gives the variation of COD, BOD_5 and TSS rejection rate, conductivity and pH as a function of pressure for the three membranes tested.

According to the data presented in Fig. 3, the rejection rates of COD, BOD_5 and TSS increase proportionally with increasing TMP, for the three membranes tested. For the 20 nm pore size membrane, the rejection rates reach 80% for COD, 84% for BOD_5 and 51% for TSS, respectively. For the 50 nm membrane, these rates are 71% for COD, 77.27% for BOD_5 and 45% for TSS, while for the 100 nm membrane, they are 68% for COD, 70.92% for BOD_5 and 41% for TSS. In addition, the rejection rate of COD, BOD_5 and TSS for the three membranes follows the following order: RUF20 > RUF50 > RUF100. These results indicate that the membrane porosity has a direct influence on the treatment efficiency and that the finer membranes have a better removal efficiency of organic pollutants and TSSs.

The results obtained in this study confirm that the TMP has an influence on the permeate flux and the discharge rates of COD, BOD_5 and TSS, which is consistent with the results of previous studies. However, it should be noted

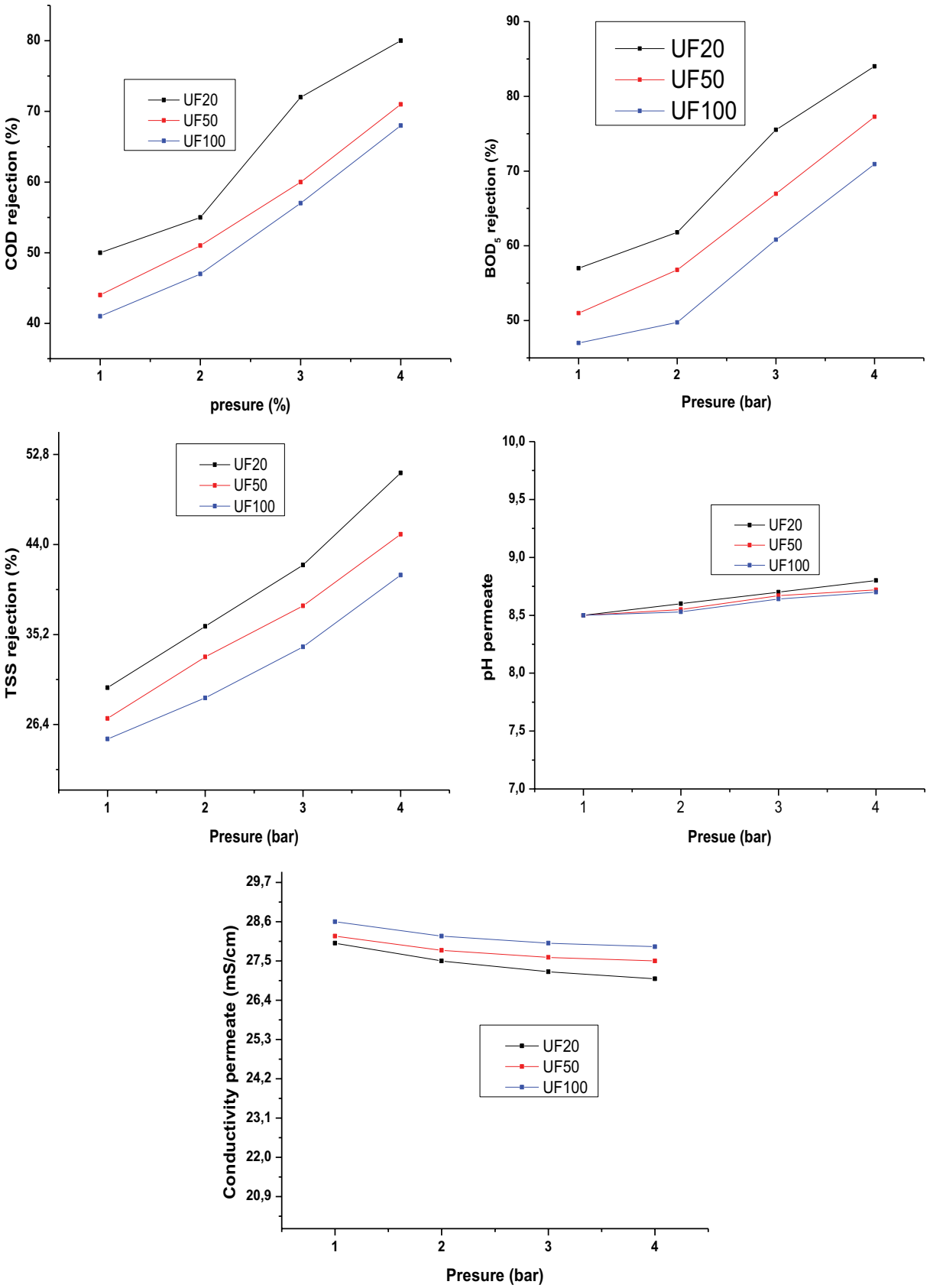

Fig. 3. Variations of chemical oxygen demand, 5-d biochemical oxygen demand and total suspended solids rejection rate. Electric conductivity and pH as a function of pressure for the three membranes.

that TMP has no impact on the conductivity of the treated solutions, since the membranes used are porous and allow mineral salts to pass through. On the other hand, a slight variation in pH was observed for the three ultrafiltration membranes [38,39].

3.2. Analysis of the fouling mechanisms of UF ceramic membranes based on Hermia and Bolton models

The identification of the fouling mechanism for the three membranes was conducted using two models: the Hermia model and the Bolton model. A comparison between these two models in describing the fouling mechanism was carried out by applying the Levenberg–Marquardt method to calculate the coefficient of determination.

3.2.1. Fouling identification: Hermia model

The fouling mode was identified and compared using the Hermia models corresponding to cake formation (cf), intermediate blocking (ib), pore constriction (pc), and complete blocking (cb), respectively [40,41]. The parameters associated with these fouling mechanisms (K_{cf}, K_{ib}, K_{pc}, and K_{cb}) were optimized using the Levenberg–Marquardt least squares method, ensuring the determination of optimal conditions for each membrane. Subsequently, we analyze the permeate flux expressions related to the four fouling mechanisms of the Hermia model, as modified by Field et al. [20]. The flux expressions mentioned by Slimane et al. [42] are summarized in Table 4.

The parameters (K_{cf}, K_{pc}, K_{ib}, and K_{cb}) associated with each fouling mechanism were optimized using the least squares method. The resulting expressions, obtained through the analytical resolution of the model, are presented in Eq. (2).

$$K_{cf} = \frac{\alpha C \mu p}{\rho_s \Delta P}, K_{ib} = \frac{C}{\rho_s h}, K_{pc} = \frac{2CJ_0^{1/2}}{\rho_s e}, K_{cb} = \frac{J_0}{\rho_s h} \quad (2)$$

Charfi et al. [40] provide a detailed description of all these parameters.

Table 4
Flux expressions of the classical single models

Model	Equations	Characteristic parameters
Cake formation (cf)	$J = \frac{J_0}{\left(2K_{cf}J_0^2 t + 1\right)^{1/2}}$	K_{cf} (s/m^2)
Intermediate blocking (ib)	$J = \frac{J_0}{K_{ib}J_0 t + 1}$	K_{ib} (m^{-1})
Pore constriction (pc)	$J = \frac{4J_0}{\left(K_{pc}J_0^{1/2} t + 2\right)^2}$	K_{pc} (m^{-1})
Complete blocking (cb)	$J = J_0 \exp\left(-K_{cb} t\right)$	K_{cb} (s^{-1})

The graph in Figs. 4–6 illustrates the variation of permeate flux over time for the three tested membranes, both as measured experimentally and as modeled using the 4 Hermia equations. This data is presented for each pressure condition. Meanwhile, Table 5 provides the values for the modeling constants related to fouling and *R*-square for each of the three membranes under the four Hermia modeling equations. These constants are shown for each pressure condition as well.

The analysis of the results revealed that the cake-forming fouling mode and intermediate blocking yielded the most favorable outcomes in terms of *R*-squared. Moreover, their modeled constants are significant and similar to those reported by Charfi et al. [40] and Kennedy et al. [43].

However, the model does not converge for the other two mechanisms, as indicated by the low *R*-squared values obtained. This suggests that the contribution of these types of fouling is negligible in our case, likely due to the small pore size of the membranes and the nature of the organic substances present in the leachate solution being treated, which promote fouling of the membrane surface [44].

The optimized parameter values indicate that the intermediate and cake-forming mechanisms may either compete or complement each other. To gain a deeper understanding of this phenomenon, flux modeling was conducted using the Bolton model.

3.2.2. Fouling identification: Bolton model

The combined models developed by Bolton et al. [22] incorporating two distinct fouling mechanisms such as cake formation and complete blocking, cake formation and intermediate blocking, complete blocking and pore constriction, and intermediate blocking and pore constriction, were also applied to consider the possibility of fouling mechanism combinations during the ultrafiltration of Oum Azza leachates.

Table 6 summarizes the flux expressions of the combined models, derived from the volume expressions previously mentioned by Slimane et al. [42].

Figs. 7–9 give the variation of permeate flux obtained experimentally and modeled using Bolton model, as a function of time in each pressure for the three tested membranes. And Table 7 gives the values of the modeling constants for fouling and *R*-squared in each pressure for the three membranes and for the Bolton model.

Figs. 7–9 and Table 7 show the experimental results of permeate flux vs. time for the three membranes. The combined models were fitting to these results, and the results show that the combined standard blocking and cake layer model did not converge.

The *R*-squared values obtained for the combined model of cake formation and complete blocking are the highest for both membranes (UF20 and UF50). However, for the UF100 membrane, the *R*-squared values are higher for the combined model of cake formation and intermediate blocking.

For the UF20 and UF50 membranes, the presence of molecules and suspended particles in the treated leachate that are similar or larger in size than the membrane pores promote complete blockage of the pores, resulting in cake formation.

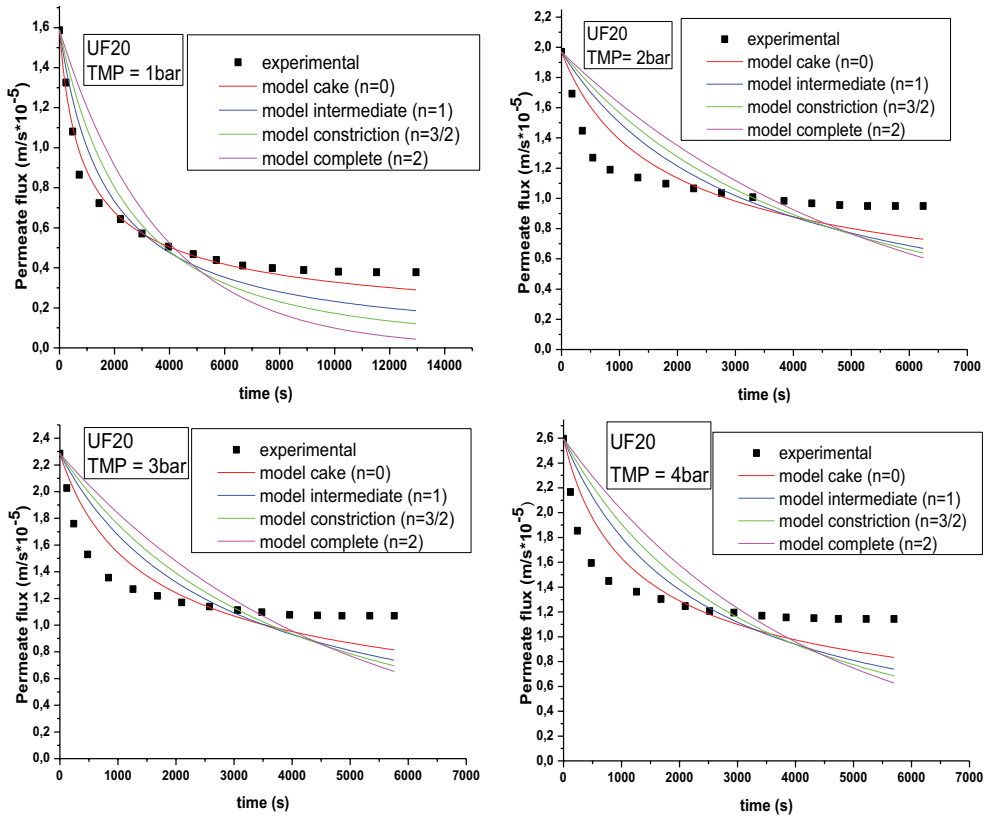

Fig. 4. Experiments and the four fouling mechanisms for the UF20 membrane in the Hermia model at different pressures.

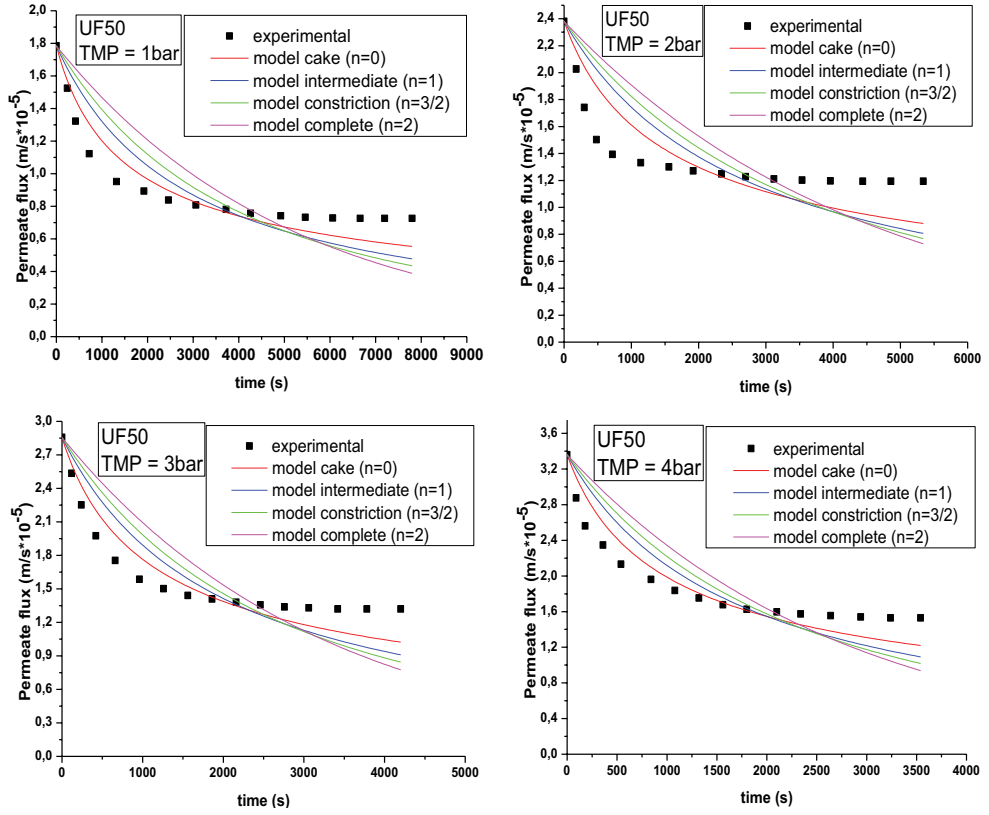

Fig. 5. Experiments and the four fouling mechanisms for the UF50 membrane in the Hermia model at different pressures.

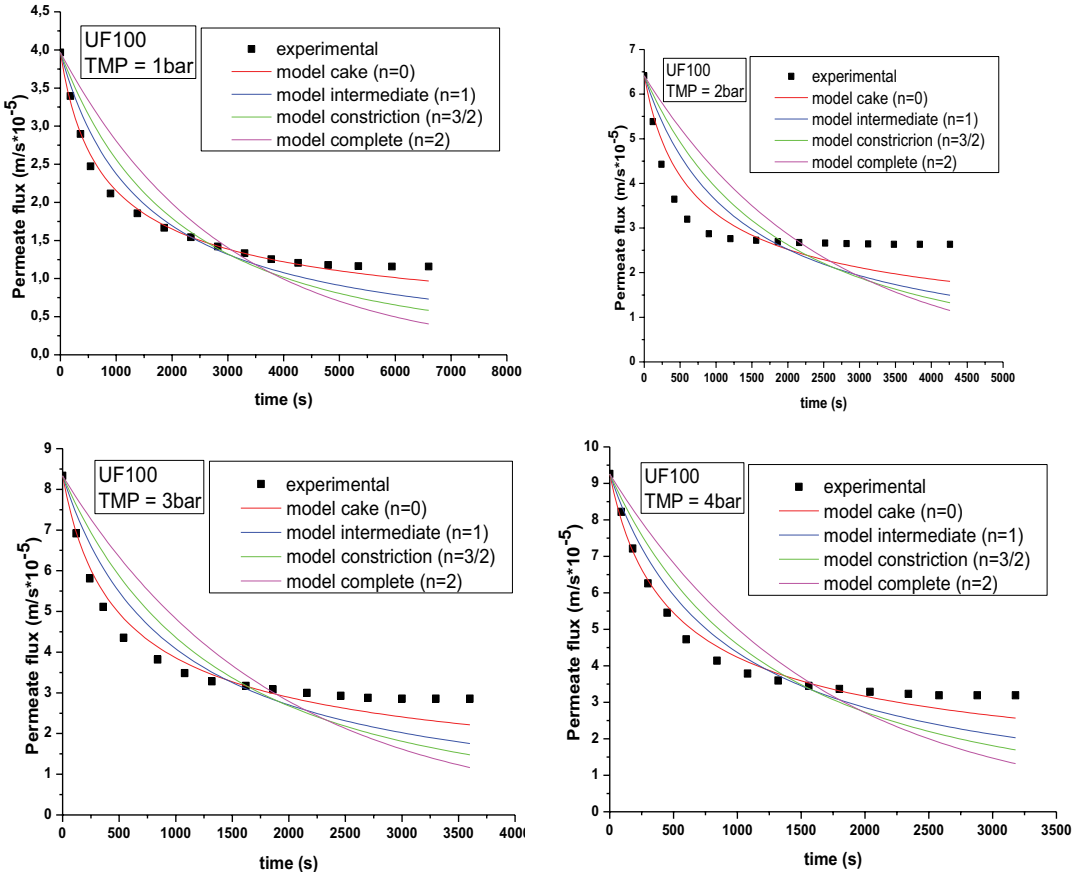

Fig. 6. Experiments and the four fouling mechanisms for the UF100 membrane in the Hermia model at different pressures.

Table 5
Fouling modeling constants for the three membranes

	P	$n = 0$	R-square	$n = 1$	R-square	$n = 1.5$	R-square	$n = 2$	R-square
UF20	1	$K_{cf} = 4.43 \cdot 10^{6}$	0.98	$K_{ib} = 36.77$	0.87	$K_{pc} = 0.101$	0.75	$K_{cb} = 2.77 \cdot 10^{-4}$	0.55
	2	$K_{cf} = 1.29 \cdot 10^{6}$	0.67	$K_{ib} = 15.8$	0.41	$K_{pc} = 0.054$	0.23	$K_{cb} = 1.88 \cdot 10^{-4}$	0.02
	3	$K_{cf} = 1.14 \cdot 10^{6}$	0.77	$K_{ib} = 15.93$	0.55	$K_{pc} = 0.058$	0.40	$K_{cb} = 2.17 \cdot 10^{-4}$	0.21
	4	$K_{cf} = 1.13 \cdot 10^{6}$	0.71	$K_{ib} = 16.99$	0.44	$K_{pc} = 0.065$	0.25	$K_{cb} = 2.84 \cdot 10^{-4}$	0.01
UF50	1	$K_{cf} = 1.89 \cdot 10^{6}$	0.88	$K_{ib} = 19.66$	0.70	$K_{pc} = 0.062$	0.55	$K_{cb} = 1.95 \cdot 10^{-4}$	0.35
	2	$K_{cf} = 1.04 \cdot 10^{6}$	0.57	$K_{ib} = 15.33$	0.25	$K_{pc} = 0.058$	0.05	$K_{cb} = 1.21 \cdot 10^{-4}$	0.02
	3	$K_{cf} = 9.92 \cdot 10^{5}$	0.87	$K_{ib} = 17.84$	0.70	$K_{pc} = 0.074$	0.57	$K_{cb} = 3.1 \cdot 10^{-4}$	0.40
	4	$K_{cf} = 8.24 \cdot 10^{5}$	0.87	$K_{ib} = 17.45$	0.70	$K_{pc} = 0.079$	0.57	$K_{cb} = 3.6 \cdot 10^{-4}$	0.40
UF100	1	$K_{cf} = 7.59 \cdot 10^{5}$	0.99	$K_{ib} = 16.89$	0.91	$K_{pc} = 0.077$	0.81	$K_{cb} = 3.45 \cdot 10^{-4}$	0.66
	2	$K_{cf} = 3.32 \cdot 10^{5}$	0.78	$K_{ib} = 12.03$	0.50	$K_{pc} = 0.07$	0.28	$K_{cb} = 4.02 \cdot 10^{-4}$	0.01
	3	$K_{cf} = 2.63 \cdot 10^{5}$	0.95	$K_{ib} = 12.49$	0.82	$K_{pc} = 0.083$	0.68	$K_{cb} = 5.46 \cdot 10^{-4}$	0.47
	4	$K_{cf} = 2.2 \cdot 10^{5}$	0.97	$K_{ib} = 12.1$	0.89	$K_{pc} = 0.087$	0.79	$K_{cb} = 6.13 \cdot 10^{-4}$	0.63

In the case of the UF100 membrane, the mechanisms of intermediate blocking and cake formation complement each other. This type of fouling occurs due to the accumulation of retained material on the membrane surface caused by concentration polarization, progressively blocking the surface pores and leading to cake formation. These findings are consistent with the work of Carbonell-Alcaina et al. [45] who also explained that concentration polarization initially decreases the permeate flux. Furthermore, membranes with smaller pores tend to retain more dissolved material, increasing the specific resistance of the cake [32,40].

Interestingly, membrane fouling decreases as the membrane pore size increases. These results align with the

Table 6
Flux expressions of the combined models

Model	Equations	Characteristic parameters
Complete-Cake (Cb-Cf)	$J=\frac{J_0}{\sqrt{1+2K_{cb}J_0^2t}}\exp\left(\left(-\frac{K_{cb}}{K_{cf}J_0^2}\right)\left(\sqrt{1+2K_{cf}J_0^2t}-1\right)\right)$	K_{cf} (s/m²) K_{cb} (s⁻¹)
Intermediate-Cake (Ib-Cf)	$J=\frac{J_0}{\sqrt{1+2K_{cf}J_0^2t}}\frac{1}{\left(1+\left(\frac{K_{ib}}{K_{cf}J_0}\right)\left(-1+\sqrt{2K_{cf}J_0^2t+1}\right)\right)}$	K_{cf} (s/m²) K_{ib} (m⁻¹)
Complete-Pore constriction (Cb-Pc)	$J=\frac{4J_0}{\left(2+K_{pc}J_0t\right)^2}\exp\left(\frac{-2K_{cb}t}{2+K_{pc}J_0t}\right)$	K_{cb} (s⁻¹) K_{pc} (m⁻¹)
Intermediate-Pore constriction (Ib-Pc)	$J=\frac{4J_0}{\left(2+K_{pc}J_0t\right)^2\left(1+\frac{2K_{ib}J_0t}{2+K_{pc}J_0t}\right)}$	K_{ib} (m⁻¹) K_{pc} (m⁻¹)

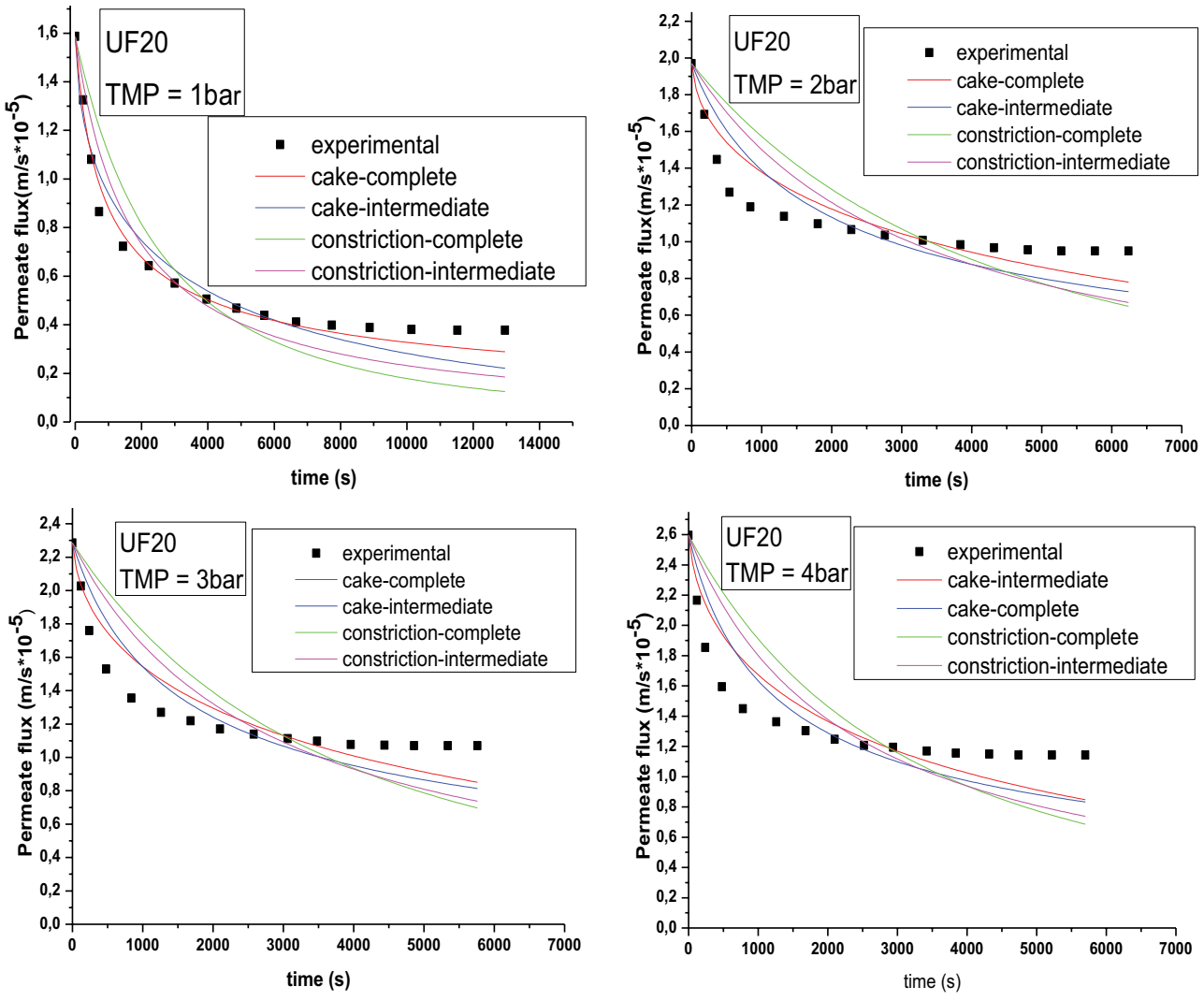

Fig. 7. Fitting of combined Bolton model to experimental results for UF20 membrane at different pressures.

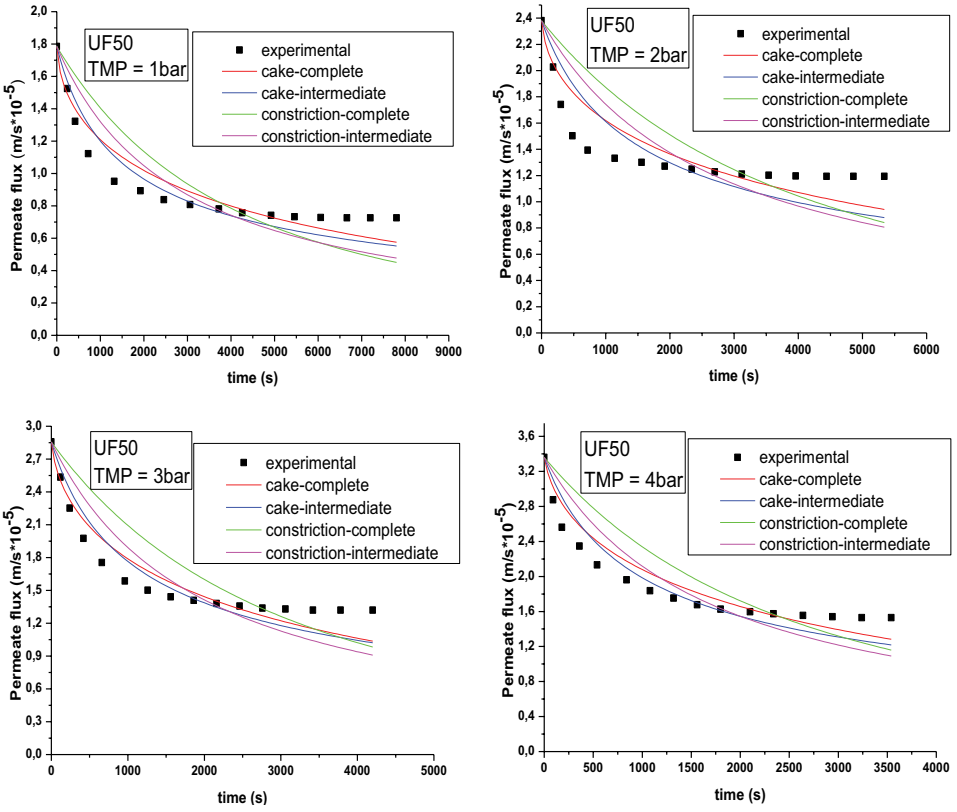

Fig. 8. Fitting of combined Bolton model to experimental results for UF50 membrane at different pressures.

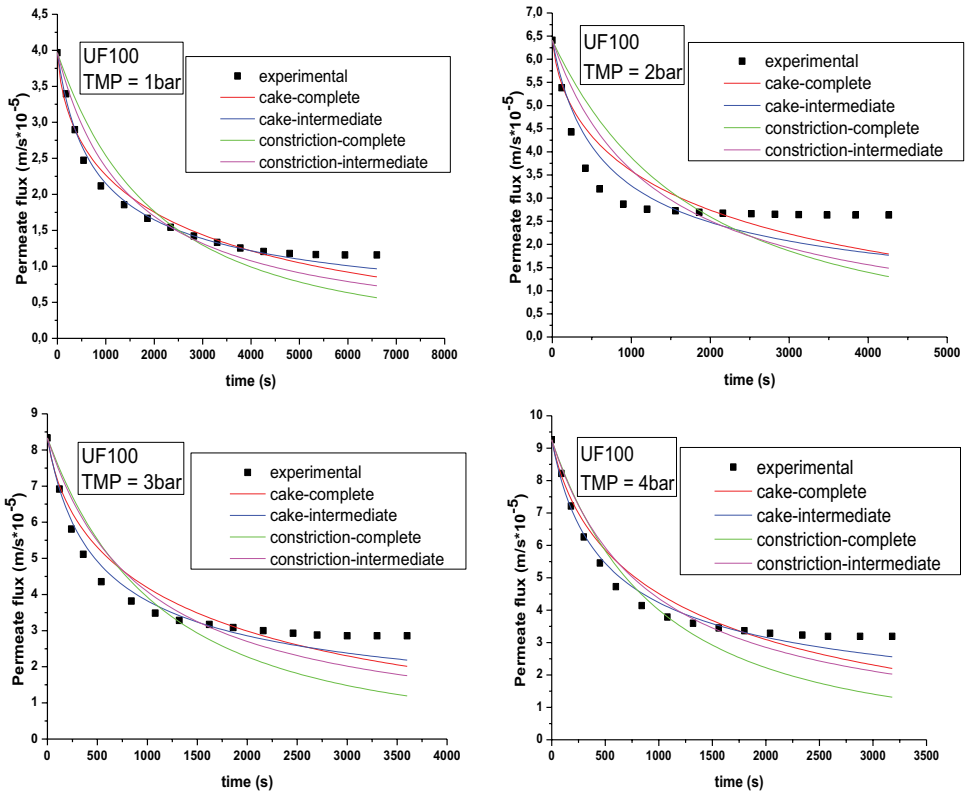

Fig. 9. Fitting of combined Bolton model to experimental results for UF100 membrane at different pressures.

Table 7
Modeling constants for the fouling of Bolton models for the three membranes

	P	K_{cf}–K_{cb}	*R*-square	K_{cf}–K_{ib}	*R*-square	K_{pc}–K_{cb}	*R*-square	K_{pc}–K_{ib}	*R*-square
UF20	1	$K_{cf} = 5.25 \cdot 10^{8}$	0.98	$K_{cf} = 4.44 \cdot 10^{6}$	0.94	$K_{pc} = 22.8$	0.73	$K_{pc} = 0.01$	0.87
		$K_{cb} = 4.53 \cdot 10^{-3}$		$K_{ib} = 0.05$		$K_{cb} = 3.34 \cdot 10^{-5}$		$K_{ib} = 36.73$	
	2	$K_{cf} = 2.95 \cdot 10^{8}$	0.78	$K_{cf} = 1.30 \cdot 10^{6}$	0.66	$K_{pc} = 11$	0.17	$K_{pc} = 0.01$	0.37
		$K_{cb} = 2.88 \cdot 10^{-3}$		$K_{ib} = 0.0317$		$K_{cb} = 2.11 \cdot 10^{-5}$		$K_{ib} = 15.8$	
	3	$K_{cf} = 1.35 \cdot 10^{8}$	0.83	$K_{cf} = 1.14 \cdot 10^{6}$	0.75	$K_{pc} = 11.9$	0.36	$K_{pc} = 0.01$	0.52
		$K_{cb} = 2.53 \cdot 10^{-3}$		$K_{ib} = 0.0266$		$K_{cb} = 9.5 \cdot 10^{-6}$		$K_{ib} = 15.93$	
	4	$K_{cf} = 5.84E7$	0.74	$K_{cf} = 1.13 \cdot 10^{6}$	0.69	$K_{pc} = 12.6$	0.20	$K_{pc} = 0.01$	0.40
		$K_{cb} = 2.18 \cdot 10^{-3}$		$K_{ib} = 0.0199$		$K_{cb} = 4.56 \cdot 10^{-6}$		$K_{ib} = 16.99$	
UF50	1	$K_{cf} = 3.78 \cdot 10^{8}$	0.88	$K_{cf} = 1.89 \cdot 10^{6}$	0.87	$K_{pc} = 13.1$	0.51	$K_{pc} = 0.01$	0.68
		$K_{cb} = 3.22 \cdot 10^{-3}$		$K_{ib} = 0.042$		$K_{cb} = 1.98 \cdot 10^{-5}$		$K_{ib} = 19.66$	
	2	$K_{cf} = 1.6 \cdot 10^{8}$	0.68	$K_{cf} = 1.04 \cdot 10^{6}$	0.53	$K_{pc} = 10.1$	0.04	$K_{pc} = 0.01$	0.20
		$K_{cb} = 2.79 \cdot 10^{-3}$		$K_{ib} = 0.0301$		$K_{cb} = 1.46 \cdot 10^{-5}$		$K_{ib} = 15.33$	
	3	$K_{cf} = 5.1 \cdot 10^{7}$	0.88	$K_{cf} = 9.92 \cdot 10^{5}$	0.86	$K_{pc} = 11.5$	0.48	$K_{pc} = 0.01$	0.68
		$K_{cb} = 2.38 \cdot 10^{-3}$		$K_{ib} = 0.0235$		$K_{cb} = 7.38 \cdot 10^{-6}$		$K_{ib} = 17.84$	
	4	$K_{cf} = 2.36 \cdot 10^{7}$	0.88	$K_{cf} = 8.24 \cdot 10^{5}$	0.86	$K_{pc} = 11.7$	0.49	$K_{pc} = 0.01$	0.68
		$K_{cb} = 2.01 \cdot 10^{-3}$		$K_{ib} = 0.0186$		$K_{cb} = 3.79 \cdot 10^{-6}$		$K_{ib} = 17.45$	
UF100	1	$K_{cf} = 2.65 \cdot 10^{7}$	0.96	$K_{cf} = 7.6 \cdot 10^{5}$	0.98	$K_{pc} = 12.3$	0.80	$K_{pc} = 0.01$	0.90
		$K_{cb} = 2.85 \cdot 10^{-3}$		$K_{ib} = 0.0333$		$K_{cb} = 1.19 \cdot 10^{-5}$		$K_{ib} = 16.89$	
	2	$K_{cf} = 8.16 \cdot 10^{6}$	0.71	$K_{cf} = 3.45 \cdot 10^{5}$	0.76	$K_{pc} = 8.77$	0.23	$K_{pc} = 0.01$	0.47
		$K_{cb} = 2.68 \cdot 10^{-3}$		$K_{ib} = 0.0279$		$K_{cb} = 9.08 \cdot 10^{-6}$		$K_{ib} = 12.09$	
	3	$K_{cf} = 2.12 \cdot 10^{6}$	0.89	$K_{cf} = 2.69 \cdot 10^{5}$	0.95	$K_{pc} = 10.9$	0.62	$K_{pc} = 0.01$	0.80
		$K_{cb} = 2.24 \cdot 10^{-3}$		$K_{ib} = 0.0213$		$K_{cb} = 5.07 \cdot 10^{-6}$		$K_{ib} = 12.49$	
	4	$K_{cf} = 8.4 \cdot 10^{5}$	0.91	$K_{cf} = 2.2 \cdot 10^{5}$	0.97	$K_{pc} = 11.2$	0.73	$K_{pc} = 0.01$	0.88
		$K_{cb} = 1.77 \cdot 10^{-3}$		$K_{ib} = 0.0175$		$K_{cb} = 3.29 \cdot 10^{-6}$		$K_{ib} = 12.1$	

findings of Gomes et al. [46]. Li et al. [47] also observed the simultaneous occurrence of intermediate blocking and cake layer formation during the ultrafiltration process of river water that underwent combined coagulation/ultrafiltration treatment under various conditions.

In conclusion, while the Hermia model displays a larger deviation from experimental values concerning fouling mechanisms and flow compared to the Bolton model, we tend to favor the Bolton model for providing a more comprehensive explanation of membrane fouling. This preference stems from the complexity of the leachate, a liquid containing various pollutants of different sizes, suggesting the involvement of multiple mechanisms in explaining fouling. The study's results indicate that membrane fouling initiates with an intermediate blockage, where particles of intermediate size partially obstruct membrane pores. This results in a gradual reduction in membrane permeability, followed by the formation of a cake in which particles or solutes accumulate on the surface of the membrane, creating a thick layer.

Moreover, the critical flow is not maintained as effectively in the modeled values as in the experimental values, which can be considered a limitation in applying the two models to real-world conditions. This discrepancy can be attributed to the surface area of the membrane used in our laboratory pilot and the high loading of the treated effluent, leading to rapid fouling of the membrane.

4. Conclusion

Leachates pose a persistent environmental problem that can cause harmful and toxic damage to human health and ecosystems. Therefore, it is crucial to treat leachates to eliminate organic pollutants and reduce salinity, thus preventing any negative impact on the environment and public health.

This study aims to investigate the efficacy of utilizing three ceramic membranes with different pore sizes (20, 50, and 100 nm) in the treatment of leachates using a semi-batch configuration at different transmembrane pressures and 2 m/s circulation velocity.

The results indicate:

- increasing TMP improves permeate flux and organic pollutant rejection for the three membranes tested;
- that the maximum rejection rates are 80%, 71% and 68% for COD, 84%, 77.27%, and 70.92% for BOD_5, and 51%, 45%, and 41% for TSS for UF20, UF50 and UF100 membranes, respectively;
- fouling analysis conducted using the Hermia and Bolton model reveals that the observed fouling is superficial for the three membranes tested;
- Hermia model, fouling in all three UF membranes is attributed to cake formation or intermediate blockage. However, the Bolton model describes fouling of the UF20 and UF50 membranes through a combined equation

that considers both cake formation and complete blockage. In contrast, fouling of the UF100 membrane is described by a combined equation that considers cake formation and intermediate blockage.

References

[1] C.P. Pereira, T. da Conceição Pereira, G. Gomes, B.R. Quintaes, D.M. Bila, J.C. Campos, Evaluation of reduction estrogenic activity in the combined treatment of landfill leachate and sanitary sewage, Waste Manage., 80 (2018) 339–348.

[2] P. Yao, Perspectives on technology for landfill leachate treatment, Arabian J. Chem., 10 (2017) S2567–S2574.

[3] T. Robinson, Removal of toxic metals during biological treatment of landfill leachates, Waste Manage., 63 (2017) 299–309.

[4] D. Zhang, R. Vahala, Y. Wang, B.F. Smets, Microbes in biological processes for municipal landfill leachate treatment: community, function and interaction, Int. Biodeterior. Biodegrad., 113 (2016) 88–96.

[5] L. Wu, L. Zhang, Y. Xu, C. Liang, H. Kong, X. Shi, Y. Peng, Advanced nitrogen removal using bio-refractory organics as carbon source for biological treatment of landfill leachate, Sep. Purif. Technol., 170 (2016) 306–313.

[6] M. Verma, R. Naresh Kumar, Can coagulation–flocculation be an effective pre-treatment option for landfill leachate and municipal wastewater co-treatment?, Perspect. Sci., 8 (2016) 492–494.

[7] Y.-n. Chen, C.-h. Liu, J.-x. Nie, X.-p. Luo, D.-s. Wang, Chemical precipitation and biosorption treating landfill leachate to remove ammonium-nitrogen, Clean Technol. Environ. Policy, 15 (2013) 395–399.

[8] Á. Anglada, A. Urtiaga, I. Ortiz, D. Mantzavinos, E. Diamadopoulos, Boron-doped diamond anodic treatment of landfill leachate: evaluation of operating variables and formation of oxidation by-products, Water Res., 45 (2011) 828–838.

[9] D. Trebouet, J.P. Schlumpf, P. Jaouen, F. Quemeneur, Stabilized landfill leachate treatment by combined physicochemical–nanofiltration process, Water Res., 35 (2001) 2935–2942.

[10] P. Yao, Perspectives on technology for landfill leachate treatment, Arabian J. Chem., 10 (2017) S2567–S2574.

[11] L.B. Chaudhari, Z.V.P. Murthy, Treatment of landfill leachates by nanofiltration, J. Environ. Manage., 91 (2010) 1209–1217.

[12] A. Majouli, S. Tahiri, S. Alami Younssi, H. Loukili, A. Albizane, Elaboration of new tubular ceramic membrane from local Moroccan perlite for microfiltration process. Application to treatment of industrial wastewaters, Ceram. Int., 38 (2012) 4295–4303.

[13] I. Jedidi, S. Saïdi, S. Khemakhem, A. Larbot, N. Elloumi-Ammar, A. Fourati, A. Charfi, A. Ben Salah, R. Ben Amar, Elaboration of new ceramic microfiltration membranes from mineral coal fly ash applied to wastewater treatment, J. Hazard. Mater., 172 (2009) 152–158.

[14] G.-T. Lim, H.-G. Jeong, I.-S. Hwang, D.-H. Kim, N. Park, J. Cho, Fabrication of a silica ceramic membrane using the aerosol flame deposition method for pretreatment focusing on particle control during desalination, Desalination, 238 (2009) 53–59.

[15] C.G. Chol, R. Dhabhai, A.K. Dalai, M. Reaney, Purification of crude glycerol derived from biodiesel production process: experimental studies and techno-economic analyses, Fuel Process. Technol., 178 (2018) 78–87.

[16] M. Lee, Z. Wu, K. Li, Advances in Ceramic Membranes for Water Treatment, A. Basile, A. Cassano, N.K. Rastogi, Eds., Advances in Membrane Technologies for Water Treatment: Materials, Processes and Applications, Woodhead Publishing Series in Energy, Woodhead Publishing, Oxford, 2015, pp. 43–82.

[17] F.P. Cuperus, H. Nijhuis, Applications of membrane technology to food processing, Trends Food Sci. Technol., 7 (1993) 277–282.

[18] E. Iritani, A review on modeling of pore-blocking behaviors of membranes during pressurized membrane filtration, Drying Technol.: An Int. J., 31 (2013) 146–162.

[19] J. Hermia, Constant pressure blocking filtration laws - application to power law non-Newtonian fluids, Chem. Eng. Res. Des., 60 (1982) 183–187.

[20] R.W. Field, D. Wu, J.A. Howell, B.B. Gupta, Critical flux concept for microfiltration fouling, J. Membr. Sci., 100 (1995) 259–272.

[21] C.-C. Ho, A.L. Zydney, A combined pore blockage and cake filtration model for protein fouling during microfiltration, J. Colloid Interface Sci., 232 (2000) 389–399.

[22] G. Bolton, D. LaCasse, R. Kuriyel, Combined models of membrane fouling: development and application to microfiltration and ultrafiltration of biological fluids, J. Membr. Sci., 277 (2006) 75–84.

[23] M.C.S. Gomes, W.M. Moreira, S.M. Paschoal, C.C. Sipoli, R.M. Suzuki, J.G. Sgorlon, N.C. Pereira, Modeling of fouling mechanisms in the biodiesel purification using ceramic membranes, Sep. Purif. Technol., 269 (2021) 118595, doi: 10.1016/j.seppur.2021.118595.

[24] W. Tomczak, M. Gryta, Application of ultrafiltration ceramic membrane for separation of oily wastewater generated by maritime transportation, Sep. Purif. Technol., 261 (2021) 118259, doi: 10.1016/j.seppur.2020.118259.

[25] O. Birrenbach, F. Faust, M. Ebrahimi, R. Fan, P. Czermak, Recovery and purification of protein aggregates from cell lysates using ceramic membranes: fouling analysis and modeling of ultrafiltration, Front. Chem. Eng., 3 (2021) 656345, doi: 10.3389/fceng.2021.656345.

[26] H. Aloulou, A. Attia, W. Aloulou, S. Chakraborty, L. Baklouti, L. Dammak, R. Ben Amar, Statistical simulation, a tool for the process optimization of oily wastewater by crossflow ultrafiltration, Membranes, 12 (2022) 676, doi: 10.3390/membranes12070676.

[27] S. Collado, D. Núñez, P. Oulego, F.A. Riera, M. Díaz, Effect of landfill leachate ageing on ultrafiltration performance and membrane fouling behaviour, J. Water Process Eng., 36 (2020) 101291, doi: 10.1016/j.jwpe.2020.101291.

[28] C. Shi, D.W. Rackemann, L. Moghaddam, B. Wei, K. Li, H. Lu, C. Xie, F. Hang, W.O.S. Doherty, Ceramic membrane filtration of factory sugarcane juice: effect of pretreatment on permeate flux, juice quality and fouling, J. Food Eng., 243 (2019) 101–113.

[29] M. Zait, S. Benalla, B. Bachiri, M. Tahaikt, D. Dhiba, A. Elmidaoui, M. Taky, Performance of three ultrafiltration ceramic membranes in reducing polluting load of landfill leachate, Desal. Water Treat., 240 (2021) 33–42.

[30] S.R. Gray, N. Dow, J.D. Orbell, T. Tran, B.A. Bolto, The significance of interactions between organic compounds on low pressure membrane fouling, Water Sci. Technol., 64 (2011) 632–639.

[31] S. Barredo-Damas, M.I. Alcaina-Miranda, A. Bes-Pia, M.I. Iborra-Clar, A. Iborra-Clar, J.A. Mendoza-Roca, Ceramic membrane behavior in textile wastewater ultrafiltration, Desalination, 250 (2010) 623–628.

[32] I. Noshadi, A. Salahi, M. Hemmati, F. Rekabdar, T. Mohammadi, Experimental and ANFIS modeling for fouling analysis of oily wastewater treatment using ultrafiltration, Asia-Pac. J. Chem. Eng., 8 (2013) 527–538.

[33] P. Mikulasek, P. Dolecek, D. Smidova, P. Pospisil, Cross flow microfiltration of mineral dispersions using ceramic membranes, Desalination, 163 (2004) 333–343.

[34] B. Wojciech, E. Celinska, R. Dembczynski, Cross-flow microfiltration of fermentation broth containing native corn starch, J. Membr. Sci., 427 (2013) 118–128.

[35] Q. Li, M. Elimelech, Organic fouling and chemical cleaning of nanofiltration membranes: measurements and mechanisms, Environ. Sci. Technol., 38 (2004) 4683–4693.

[36] M.Z. Avdicevic, K. Kosutic, S. Dobrovic, Effect of operating conditions on the performances of multichannel ceramic UF membranes for textile mercerization wastewater treatment, Environ. Technol., 38 (2017) 65–77.

[37] H. Zhou, D.W. Smith, Advanced technologies in water and wastewater treatment, J. Environ. Eng. Sci., 1 (2002) 247–264.

[38] S. Renou, S. Poulain, J.G. Givaudan, P. Moulin, Amelioration of ultrafiltration process by lime treatment: case of landfill leachate, Desalination, 249 (2009) 72–82.

[39] Y.D. Xu, D.B. Yue, Y. Zhu, Y.F. Nie, Fractionation of dissolved organic matter in mature landfill leachate and its recycling by ultrafiltration and evaporation combined processes, Chemosphere, 64 (2006) 903–911.
[40] A. Charfi, N. Ben Amar, J. Harmand, Analysis of fouling mechanisms in anaerobic membrane bioreactors, Water Res., 46 (2012) 2637–2650.
[41] F.Z. Addar, S. Qaid, H. Zeggar, H. El Hajji, M. Tahaikt, A. Elmidaoui, M. Taky, Ultrafiltration of Moroccan Valencia orange juice: juice quality, optimization by custom designs and membrane fouling, SAFER, 11 (2023), doi: 10.7770/safer-V11N1-art2722.
[42] F.Z. Slimane, F. Ellouze, N. Ben Amar, Fouling mechanism and screening of backwash parameters: seawater ultrafiltration case, Environ. Eng. Res., 24 (2019) 298–308.
[43] M.D. Kennedy, J. Kamanyi, B.G.J. Heijman, G. Amy, Colloidal organic matter fouling of UF membranes: role of NOM composition & size, Desalination, 220 (2008) 200–213.
[44] B. Qi, J. Luo, G. Chen, X. Chen, Y. Wan, Application of ultrafiltration and nanofiltration for recycling cellulase and concentrating glucose from enzymatic hydrolyzate of steam exploded wheat straw, Bioresour. Technol., 104 (2012) 466–472.
[45] C. Carbonell-Alcaina, M.J. Corbaton-Baguena, S. Alvarez-Blanco, M.A. Bes-Pia, J.A. Mendoza-Roca, L. Pastor-Alcaniz, Determination of fouling mechanisms in polymeric ultrafiltration membranes using residual brines from table olive storage wastewaters as feed, J. Food Eng., 187 (2016) 14–23.
[46] M.C.S. Gomes, P.A. Arroyo, N.C. Pereira, Influence of oil quality on biodiesel purification by ultrafiltration, J. Membr. Sci., 496 (2015) 242–249.
[47] R. Li, B. Gao, W. Wang, Q. Yue, Y. Wang, Floc properties and membrane fouling in coagulation/ultrafiltration process for the treatment of Xiaoqing River: the role of polymeric aluminum-polymer dual-coagulants, Chemosphere, 243 (2020) 125391, doi: 10.1016/j.chemosphere.2019.125391.